Int. J. Electrochem. Sci., 12 **(2017)** 5392 – 5403, doi: 10.20964/2017.06.06

International Journal of ELECTROCHEMICAL SCIENCE
www.electrochemsci.org

Preparation of a Zinc Oxide-Reduced Graphene Oxide Nanocomposite for the Determination of Cadmium(II), Lead(II), Copper(II), and Mercury(II) in Water

Wei Liu[*]

School of Architecture, Chang'an University, Xi'an, 710064, P. R. China.
[*]E-mail: cauliuwei@chd.edu.cn

Received: 26 November 2016 / *Accepted:* 18 March 2016 / *Published:* 12 May 2016

An effective electrocatalyst was generated through the hybridization of graphene with ZnO. First, a proper amount of graphene oxide was used to cover the ZnO nanoparticles. Then, the composite of ZnO and graphene (ZnO/RGO) was produced through the in situ reduction of graphene oxide. The obtained ZnO/RGO composite was employed to determine Cu(II), Cd(II), Hg(II) and Pb(II) in aqueous solutions. The limits of detection for Cu(II), Cd(II), Hg(II) and Pb(II) were measured to be 0.04 μM, 0.03 μM, 0.06 μM and 0.03 μM, respectively, which are remarkably lower than the guideline values set by the World Health Organization (WHO).

Keywords: Zinc oxide; Graphene; Electrochemical sensor; Mercury; Square wave stripping voltammetry

1. INTRODUCTION

Owing to their toxicity, even in the trace amounts, towards human health, heavy metals are remarkably detrimental pollutants. Hence, the development of a quick and facile analytical approach with sensitivity to detect and monitor environmental contaminants in water is essential. So far, various mature techniques have been reported to determine heavy metal ions, involving inductively coupled plasma mass spectrometry, inductively coupled plasma atomic emission spectrometry and atomic absorption spectroscopy. Nevertheless, these reported spectrometric approaches are not appropriate for in situ determination, as the employed instruments are sophisticated, laborious, and expensive. In comparison, electrochemical techniques, which can act as alternatives to the spectroscopic methods, have been considered as effective approaches for the detection of heavy metal ions, owing to their characteristics of low cost, short analysis time, outstanding portability and sensitivity. Particularly,

among these electrochemical approaches, electrochemical stripping voltammetric analysis is a powerful tool to analyze metal ions, which can detect several metal ions simultaneously with high sensitivity [1-5]. The efficiency of the accumulation of the target analytes has been enhanced remarkably by electrodes with chemical modification, which has been further developed for anodic stripping voltammetry to detect heavy metal ions as a promising and efficient approach. Moreover, nanostructured materials are significant in the modification of electrodes to electrochemically detect heavy metal ions, as these materials exhibit specific chemical, electronic, mechanical and thermal characteristics compared to traditional materials [6].

Due to the high surface area, unique electronic transport properties and outstanding electrocatalytic activities [7], graphene, which is a "star" material, has been developed to construct electrochemical sensors as a potential nanoelectrocatalyst. Moreover, graphene applied in electrochemistry is mostly produced through reducing graphene oxide. In general, the synthesized graphene possesses diverse functional groups, including carboxyl and hydroxyl groups, which facilitate the adsorption of heavy metal ions [8]. Nevertheless, the as-prepared graphene sheets tend to undergo non-reversible agglomeration and even generate graphite through restacking when drying dispersions of graphene [9-11], due to the π–π stacking interactions and the van der Waals forces among individual graphene sheets. The agglomeration of graphene sheets can be decreased or inhibited through the combination of nanoparticles and the graphene sheets [12]. In recent years, various nanosensors based on graphene have been developed to electrochemically detect heavy metal ions, including conducting polymers [13, 14] and metal nanoparticle-based graphene [15]. Nevertheless, only a few papers have reported the use of metal oxide nanoparticle-decorated graphene to detect heavy metal ions.

ZnO, which is one of the most promising semiconductors, exhibits a hexagonal wurtzite structure with a broad band gap of 3.37 eV as well as a high exciton binding energy of 60 meV, which has been widely applied in various areas, such as catalysis, sensors, photonic detectors, photovoltaics, optoelectronic devices, and polarized light emitting devices [16]. Thus far, numerous ZnO materials with diverse single-crystal forms have been synthesized, such as thin films [17] as well as numerous one-dimensional morphologies including nanowires [18], nanorods [19] and nanobelts [20]. In particular, these nanostructures exhibit high specific surface areas and excellent mechanical stabilities, which prompt them to be appropriate candidates for the design of sensors [21] and the modification of electrodes [22].

However, only a few papers have reported electrochemical sensors that selectively and simultaneously detect various target metal ions, whereas numerous papers have reported the use of electrochemical sensors for detecting heavy metal ions. Herein, an electrochemical platform was fabricated through the combination of ZnO with graphene to simultaneously detect Cd(II), Cu(II), Hg(II) and Pb(II) in solution through square-wave anodic stripping voltammograms (SWASV). The ZnO NPs used here not only prevent the aggregation of graphene but also serve as an electrochemical catalyst for the detection of heavy metal ions. Hence, the glassy carbon electrode modified with ZnO and RGO exhibited an enhanced sensing capacity compared to bare ZnO or graphene. In addition, a broad potential gap was observed among the stripping peaks in the simultaneous detection of diverse heavy metal ions, which indicates that no interference existed between each ion. Therefore, our work

demonstrates that metal nanoparticles are excellent candidates for modifications of commercial electrode surfaces and could be potentially applied to real water pollution monitoring applications.

2. EXPERIMENTS

2.1. Chemicals

Zinc nitrate hexahydrate ($Zn(NO_3)_2 \cdot 6H_2O$) and a hydrazine solution (25% in water) were purchased from commercial sources. Acetate buffer solutions (0.1 M) at various pH were produced through mixing stock solutions containing 0.1 M NaAc and HAc, and the phosphate buffer solutions (PBS, 0.1 M) were produced by mixing stock solutions containing 0.1 M H_3PO_4, KH_2PO_4 and NaOH. The graphene oxide powder was commercially available from JCANANO. In this work, Milli-Q water (18.2 MΩ cm) was employed in all the experiments.

2.2. Characterizations

XRD (D8-Advanced, Bruker, Germany) was employed with Cu Ka radiation to record X-ray diffraction patterns in a 2θ range from 5° to 90°. Scanning electron microscopy (SEM, S-4900, Hitachi High Technologies Corporation, Japan) was used to characterize the surface morphologies of the samples. A Raman microprobe (Renishaw RM1000) was utilized to collect Raman spectroscopy at room temperature with a laser wavelength of 514 nm.

2.3. Preparation of Modified Electrode

The preparation of the ZnO/RGO nanocomposite was achieved according to a previous report [23]. To perform the electrochemical investigation, a GCE was polished by an alumina-water slurry and rinsed with water. In the case of the surface modification of the electrode, 8 μL of the dispersion of the catalyst at a concentration of 0.5 mg/mL was deposited on the surface of the GCE. Then, it was dried at room temperature. A CH Instruments 660A electrochemical workstation (CHI-660A, CH Instruments, Texas, USA) was employed to carry out the electrochemical measurements, where a three-electrode system was used. A platinum wire and Ag/AgCl with KCl (3 M) were utilized as the auxiliary electrode and reference electrode, respectively.

2.4. Cd(II), Pb(II), Cu(II), and Hg(II) Detection

To detect Cu, Cd, Hg and Pb under optimal conditions, SWASV was employed, where Cd, Cu, Hg and Pb were deposited through the reduction of Cu(II), Cd(II), Hg(II) and Pb(II) in 0.1 M NaAc-HAc solution (pH 5.0) for 150 s with a potential of -1.0 V. The anodic stripping of the electrodeposited metal, which was the reoxidation of metal into metal ions, was performed with a potential in the range of -1.0 to 0.5 V under the parameters described below: amplitude, 25 mV; increment potential, 4 mV;

frequency, 15 Hz. The same experimental conditions were employed to perform the selective and simultaneous detection of Cd(II), Cu(II), Hg(II) and Pd(II).

3. RESULTS AND DISCUSSION

The SEM images of ZnO and the nanocomposite of ZnO and RGO synthesized in one-pot are illustrated in Figure 1. In Figure 1A, a rod-shaped structure with an average length of 1.3 □M was observed in the as-synthesized ZnO in the absence of GO. In addition, in Figure 1B, it is obvious that a similar structure was obtained when the ZnO nanorods were deposited on the surface of the RGO sheets. In Figure 1B, it can be clearly seen that a large number of ZnO nanorods grew on the surface of the RGO sheet. Furthermore, the ZnO nanorods occupy the space between two RGO sheets as well, constructing a sandwich-like structure. This composite structure prevents the RGO sheets from stacking [24].

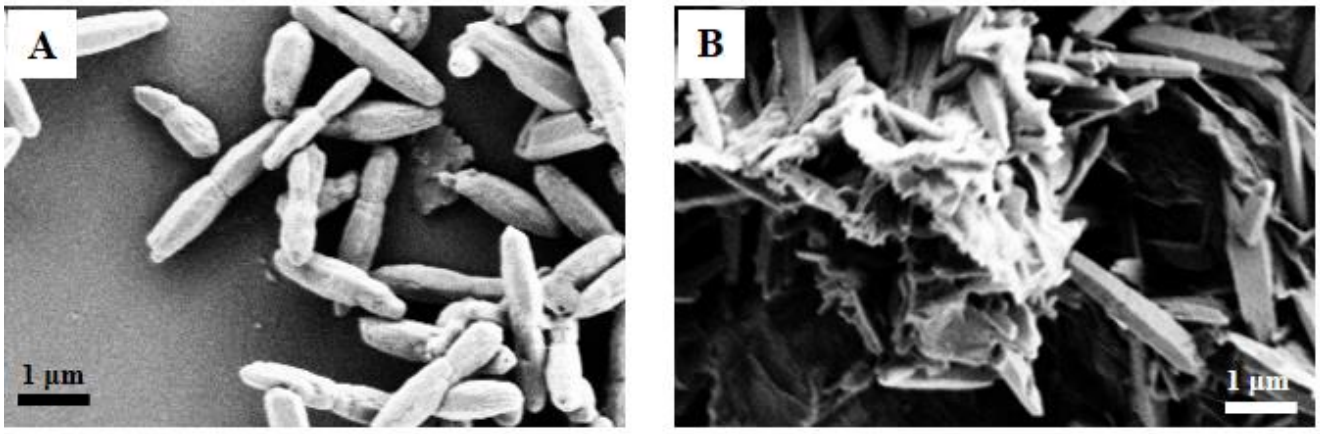

Figure 1. SEM images of ZnO nanorods (A) and ZnO/RGO (B) nanocomposite.

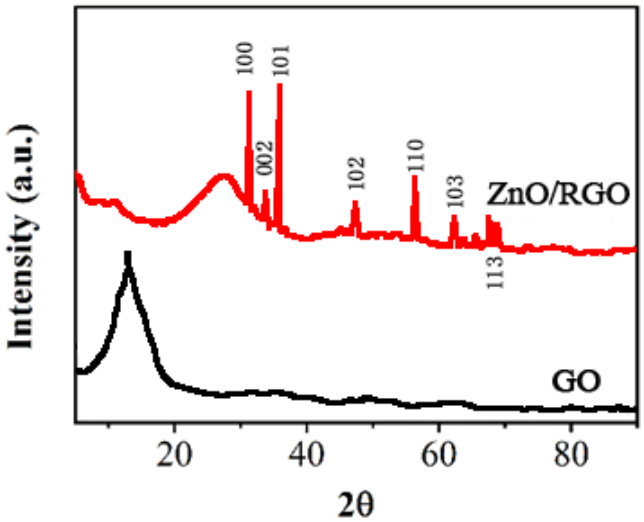

Figure 2. Structural analysis of GO and ZnO/RGO nanocomposite.

Structural analysis of GO and ZnO/RGO nanocomposite were obtained by XRD, and the patterns were demonstrated in Fig. 2. As shown in the ZnO/RGO pattern, characteristic peaks emerged at 31.4 ^{o}C, 34.2 ^{o}C, 35.7 ^{o}C, 47.4 ^{o}C, 56.2 ^{o}C, 62.5 ^{o}C and 67.4 ^{o}C are ascribed to the (100), (002), (101), (102), (110), (103) and (113) phases of hexagonal wurtzite ZnO (JCPDS 36-1451). It is worth noting that, in the case of GO pattern, a sharp peak at 11.2° was observed. It is related to the (001) plane of GO [25]. Differently, a broad diffraction peak centered at 26.4° instead of 11.2° emerged in the ZnO/RGO pattern. This further indicates that GO was reduced under the hydrothermal condition.

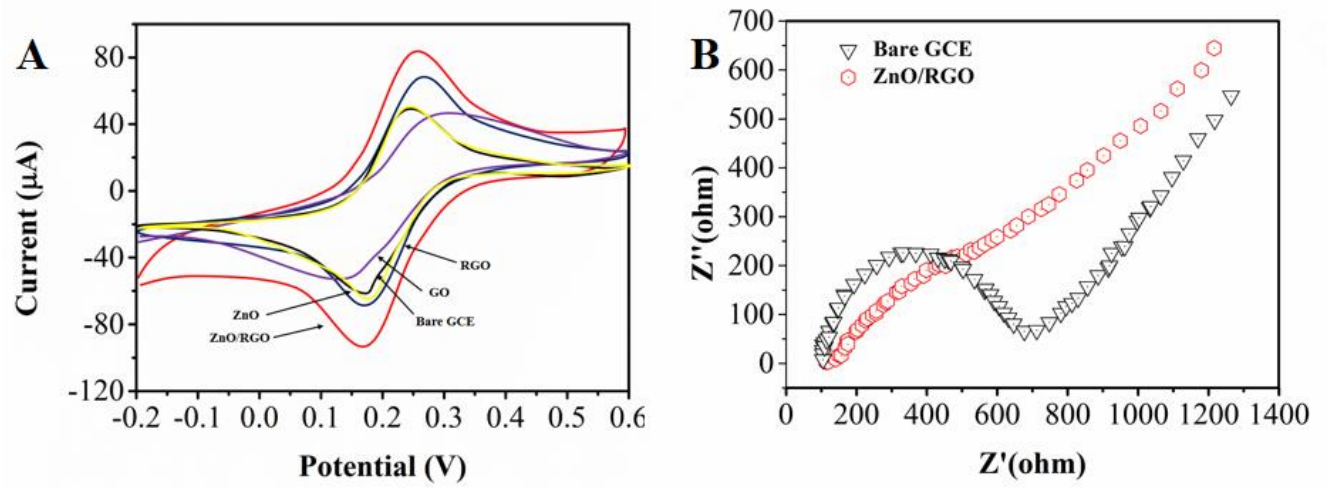

Figure 3. Cyclic voltammograms results of the bare GCE, graphene oxide, reduced graphene oxide, ZnO nanoparticle, and ZnO/RGO nanocomposite modified GCE (A); Nyquist plot of the electrochemical impedance spectra of the bare GCE and ZnO/RGO nanocomposite modified GCE (B) in a $Fe(CN)_6^{3-/4-}$ redox couple containing $Fe(CN)_6^{3-/4-}$ (5 mM) mixing with KCl (0.1 M).

The $Fe(CN)_6^{3-/4-}$ redox couple ($Fe(CN)_6^{3-/4-}$ with a concentration of 5 mM in a 0.1 M KCl solution) was utilized to measure the cyclic voltammetric response of graphene oxide and the ZnO/RGO-modified GCE nanocomposite. For comparison, the bare GCE, ZnO nanoparticles and reduced graphene oxide modified GCE were tested as well, and all results are shown in Figure 3. As shown, no obvious anodic or cathodic peaks were observed on the graphene oxide modified electrode, which is completely different from the bare GCE. This can be attributed to the functional groups in graphene oxide, e.g., hydroxyl, epoxy and carboxyl groups [26, 27]. All these groups have negative effects on the electron-transfer and mass-transfer processes, and thus, $Fe(CN)_6^{3-}$ was inhibited to be diffused onto the surface of the electrode. However, owing to the large 2-D electrical conductivity of GO, a well-defined peak was obtained on the electrode that was modified by reduced graphene oxide. For the ZnO nanoparticle modified electrode, a similar current response was observed as the bare GCE; however, the peak separation was significantly increased, suggesting a lower electron-transfer rate on the electrode surface. This is caused by the attachment of ZnO to the GCE surface. In the case of the ZnO/RGO nanocomposite electrode, it showed the highest current, indicating that better electrochemical catalytic behavior was achieved and that necessary additional conduction pathways on the electrode surface were obtained by the combination of ZnO nanoparticles and reduced graphene oxide. Moreover, the electron-transfer process was enhanced on the surface of the modified electrode.

As shown in the cyclic voltammograms, the ZnO/RGO electrode showed the largest capacitive current compared with the other electrodes, which agrees with a previous report. Thus, the obtained ZnO/RGO nanocomposite could have great potential application in electrochemical supercapacitors [28]. Warburg impedance at 45° was also observed for all the electrodes of interest. The R_{ct} value for the ZnO/RGO electrode was less than that for the bare GCE.

The interface properties of the electrodes were evaluated by electrochemical impedance spectroscopy (EIS), and the results are shown in Figure 3B. Normally, in the lower frequency range of the Nyquist plot, the linear part is ascribed to a diffusion-limited process, while in the higher frequency range, the semicircle portion is related to the electron-transfer resistance (R_{et}) [29]. In Figure 4B, the R_{et} value of the bare GCE is approximately 700 Ω. After modifying with the ZnO/RGO nanocomposite, the R_{et} value of semicircle decreased significantly, and a straight line was observed. This reveals that the electron-transfer process was remarkably improved on the surface of the electrode, which is consistent with the results from the cyclic voltammogram.

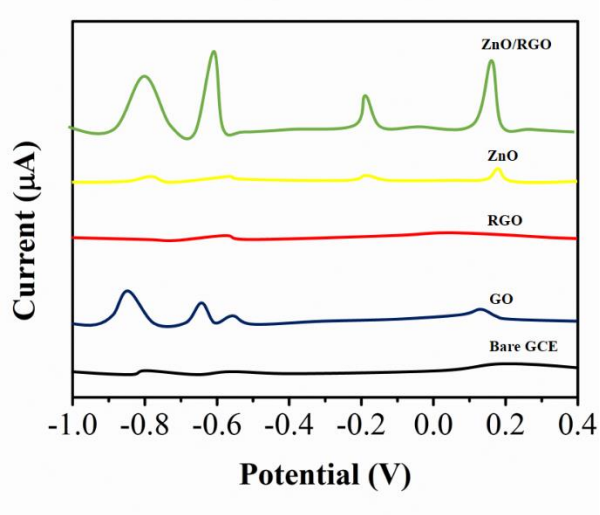

Figure 4. SWASV results of Cu(II), Cd(II), Hg(II) and Pb(II) on bare GCE, graphene oxide, reduced graphene oxide, ZnO nanoparticle and ZnO/RGO nanocomposite (pink line) modified GCE in Cd(II), Pb(II), Cu(II), and Hg(II) solution (0.5 μM mixing with acetate buffer (pH=5.0)) with a concentration of 0.1 M. Deposition potential: −1.0 V; deposition time: 150 s; amplitude: 25 mV; increment potential: 4 mV; frequency: 15 Hz; vs Ag/AgCl.

The SWASV results of the bare GCE, graphene oxide, reduced graphene oxide, ZnO nanoparticle, and ZnO/RGO-modified GCE were also obtained and are presented in Figure 4. The identification potentials of Cu(II), Cd(II), Hg(II) and Pb(II) were −0.109, -0.774, 0.24 V and −0.578, respectively. As the figure suggests, when the GCEs were measured at −1.0 V for 150 s in each solution (0.5 μM Cu(II), Cd(II), Hg(II) and Pb(II) of each mixed with 0.1 M acetate buffer (pH=5.0)), no obvious peaks emerged for the bare GCE and the GCE modified with the reduced graphene oxide, while very weak peaks were obtained on the ZnO nanoparticle modified GCE. In addition, in the case of the ZnO/RGO nanocomposite modified electrode, sharp peaks and high peak current responses to four metal ions were observed. This strongly reveals that the modification of the ZnO/RGO

nanocomposite on the GCE gave positive effects on the processes of Cu(II), Cd(II), Hg(II) and Pb(II) accumulating on the surface of the electrode. Nevertheless, due to the functional groups on the surface of the graphene oxide, sharp peaks for Cd(II) and Pb(II) were observed. It was found that the adsorbed metal ions were difficult to be removed because those functional groups can act as anchor sites to strongly capture the metal ions onto the surface of graphene oxide. This can be attributed to the well-organized accumulation of metal ions close to the electrode surface by complexation reactions [30]. Therefore, the electrode modified by graphene oxide is not reusable and therefore is not available for practical application. It is noteworthy that the ZnO-modified electrode also showed four weak peaks. This may be caused by the large sizes of ZnO nanoparticles that grew from small ones under the heating conditions as a result of the Ostwald ripening effect [31]. Apparently, ZnO nanoparticles are of great importance in the reoxidizing process of metal ions.

The determination maximum of heavy metal ions (0.5 μM Cu(II), Cd(II), Hg(II) and Pb(II)) on the ZnO/RGO-modified GCE were obtained by optimizing the voltammetric parameters, including the deposition potential, deposition time, pH value and supporting electrolytes. For instance, Cd(II) and Cu(II) solutions were chosen to optimize the deposition potential, deposition time and pH value. Three diverse electrolytes, 0.1 M NH_4Cl-HCl solution, acetate buffer and phosphate buffer, were employed to study the voltammetric behaviors of 4 target metal ions. The pH value of each solution was adjusted to 5.0, and the test results are shown in Figure 5A. Three peaks, not including Pb(II), were observed in the case of the NH_4Cl-HCl and phosphate buffer solution. However, in the case of the acetate buffer solution, four well-defined voltammetric peaks in response to the target metal ions were observed. Thus, 0.1 M acetate buffer solution (pH = 5.0) was employed in the following experiments.

The effect of pH is of great importance and should be selected properly. The voltammetric responses to pH were studied in a 0.1 M acetate buffer solution, where the pH ranged from 6.0 to 3.0. As demonstrated in Figure 5B, an increase of the peak current of Cd(II) occurred when the pH was changed between 3.0 and 5.0, where a maximum was achieved at a pH value of 5.0, and the peak current decreased when the pH increased beyond 6.0. Meanwhile, an obvious increase of the peak current of Cu(II) occurred when the pH was changed between 3.0 and 5.0, and then, the increase became less beyond a pH value of 6.0. Complexation and electrostatic attraction mechanisms can attribute to an increase of the peak current as the pH changes between 3.0 and 5.0. It is believed that groups, such as hydroxyl and carboxylic, on the surface of the carbon nanotubes are the same as those on the surface of graphene, which act as active sites to anchor heavy metal ions and possibly possess p*K*a values between 3 and 5. At pH values higher than 4, the decrease in the anodic peak current may be due to the hydrolysis of cations [30]. Therefore, the stripping measurements were conducted in a 0.1 M acetate buffer solution at a pH value of 5.0.

In the testing of the stripping analysis, achieving the best sensitivity may require an adequate deposition potential. Therefore, when the pH of the 0.1 M acetate buffer solution was 5.0, the relationship between peak current and deposition potential was investigated after 150 s accumulation, where the potential was changed from -1.4 to 0 V. The results are exhibited in Figure 5C. Increases of the stripping peak currents of Cu(II) and Cd(II) were observed when the potential changed from -1.0 to 0 V, and the value of the peak current of Cu(II) became the highest at a potential of -1.0 V. However, the response of the peak current decreased for Cu(II) and Cd(II) when the deposition potential was

lower than -1.0 V. Because formed H_2 can compete with the codeposition of metal ions when the real samples are analyzed, even though more negative potentials can lead to higher peak currents for Cd(II), a potential of -1.0 V was selected as the best deposition potential in the subsequent experiments. Various standard potentials can possibly lead to different performances for the different metals.

Because there were correlations between the sensitivity and detection limit with deposition time, different deposition times were investigated in this work. The relationships between the deposition time and the peak currents of 4 target metal ions are shown in Figure 5D. Due to the increase of the amount of analytes on the functionalized surface of the electrode, increasing the deposition time between 10 and 150 s enhanced the stripping peak currents of both Cu(II) and Cd(II). Saturation on the surface at high amounts of metal ions will make the upper limit of detection lower even though the increase of the deposition time can improve the sensitivity. Thus, a deposition time of 150 s was selected to obtain a wider range of response and a lower limit of detection.

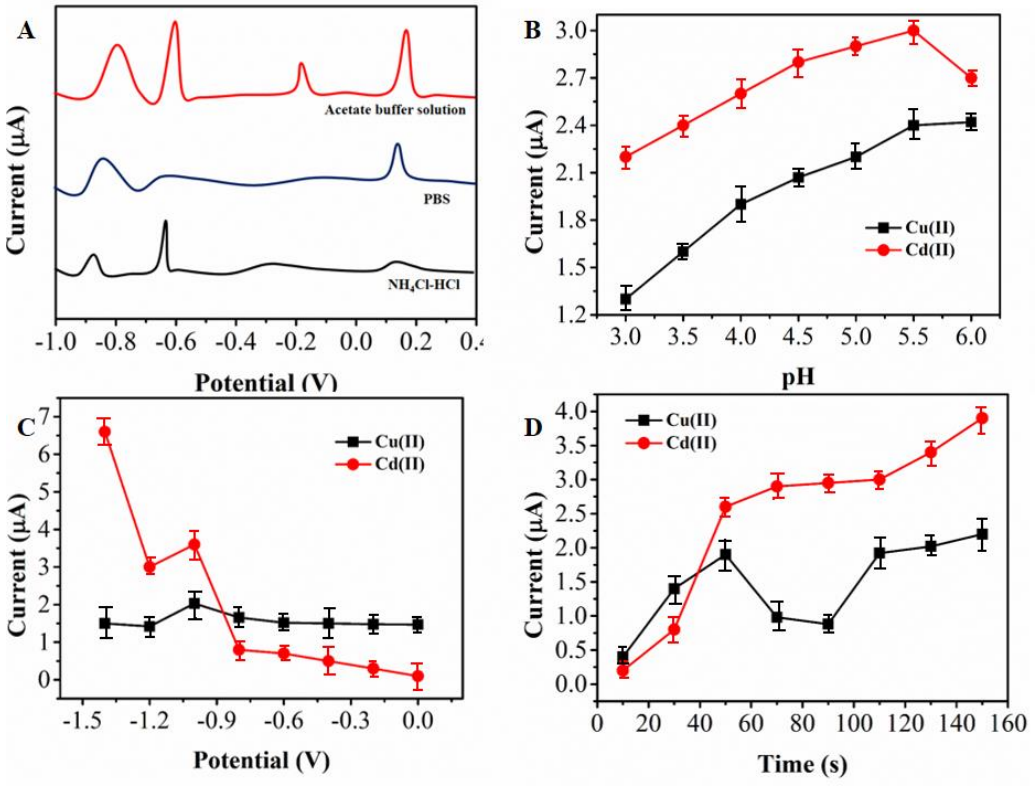

Figure 5. Optimized experimental conditions. Effect of (A) the supporting electrolytes; (B) pH value; (C) the deposition potential and (D) the deposition time on the voltammetric response of the ZnO/RGO nanocomposite modified GCE.

SWASV was employed to determine Hg(II) and Cu(II) at the electrode of ZnO/RGO individually and simultaneously under the optimized experimental conditions. The SWASV responses for Hg(II) are shown in Figure 6A with different concentrations of Hg(II) [32-35]. Excellent peaks were obtained with concentrations between 0.2 and 0.6 μM, where these peaks were in proportion to

the Hg(II) concentration. The linear equation was $i = 0.877 + 2.754c$ with a correlation coefficient of approximately 0.998, and the tested LOD was 0.07 μM. As depicted in Figure 4B, the SnO_2/rGO electrode had SWASV responses to Cu(II) in a concentration range of 0.1 to 1.3 μM. The linear fit equation was $i = 1.41 + 4.851\ c$ with a correlation coefficient of approximately 0.996, and the tested LOD was 0.04 μM. As depicted in Figure 6C, excellent Cu(II) peaks were obtained during the simultaneous analysis of Hg(II) and Cu(II). Meanwhile, the Hg(II) stripping peaks showed poor structure. A Cu-Hg intermetallic compound was formed, which lead to this result. As illustrated in Figure 6D, the calibration plots showed good linearity for Hg(II) between 0.4 and 1.2 μM, while the linearity for Cu(II) was good between 0.2 and 0.6 μM. The linear fit equations were $i = 0.724 + 2.662\ c$ and $i = 1.36 + 9.241\ c$ with correlation coefficients of approximately 0.984 and 0.995, respectively, and the tested LODs were 0.07 and 0.01 μM for Hg(II) and Cu(II), respectively. The sensing performance of the proposed sensor was compared with recently reported sensors, as shown in Table 1.

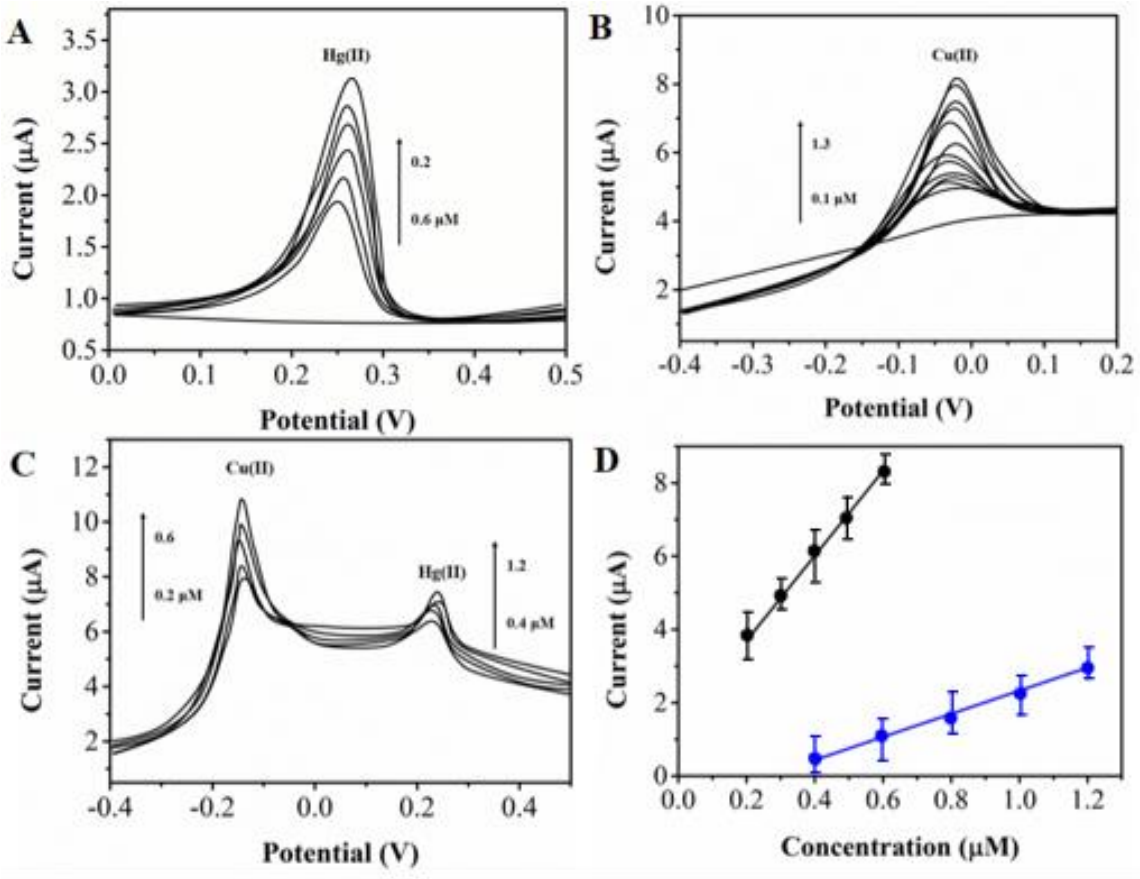

Figure 6. SWASV response of GCE functionalized by the nanocomposite of ZnO/RGO for isolated analysis of (A) Hg (II) at the concentration ranging from 0.2 to 0.6 μM and (B) Cu (II) at the concentration ranging from 0.1 to 1.3 μM. (C) SWASV response of GCE functionalized by the nanocomposite of ZnO/RGO for the simultaneously analysing Hg(II) and Cu(II)with a concentration of 0.4 to 1.2 μM and 0.2 to 0.6 μM for Hg(II) and Cu(II), respectively. (D) The individual calibration curves of Hg (II) and Cu (II).

Table 1. Performance comparison of the ZnO/RGO/GCE with for Hg(II) and Cu(II) detection.

Electrode	Linear range		Detection limit		Reference
	Hg (II)	Cu(II)	Hg (II)	Cu(II)	
G-Nafion/Bi/GCE	0.8-1.9 μM	0.05-0.5 μM	0.04 μM	0.01 μM	[13]
Nafion/Bi/NMC/GCE	0.5-1.5 μM	0.1-3 μM	0.005 μM	0.02 μM	[36]
MWCNTs-Nafion/Bi/GCE	0.1-0.6μM	1.0 -2.0 μM	0.02 μM	0.2 μM	[37]
GNFs-Nafion/Bi/GCE	0.5-1.8 μM	0.1-1.0 μM	0.05 μM	0.03 μM	[38]
OMC/Nafion/GCE	0.2-1.0 μM	1.5 -5 μM	0.03 μM	0.5 μM	[39]
ZnO/RGO	0.4-1.2 μM	0.4-1.2 μM	0.07 μM	0.01 μM	This work

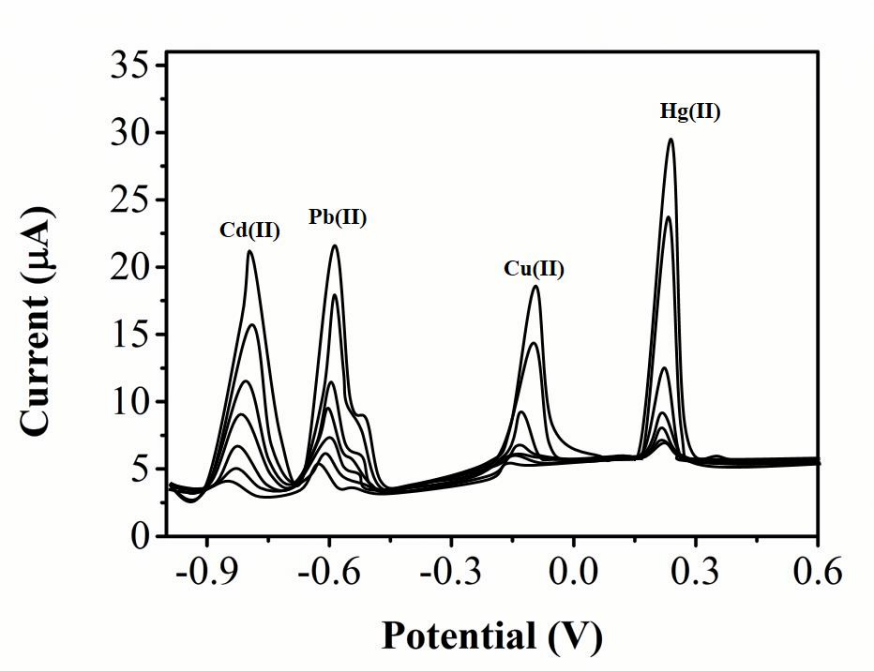

Figure 7. SWASV response of the GCE functionalized by ZnO/RGO nanocomposite for simultaneously analysing Hg (II), Pb (II), Cd (II) and Cu (II) at the concentration ranging from 0 to 1.3μM for every metal ion.

In Figure 7, under optimized experimental conditions, the SWASV analysis to analyze Cu(II), Cd(II), Pb(II) and Hg(II) upon increases in the concentrations were typically recorded by the electrode modified with the nanocomposite of ZnO/reduced graphene oxide. The well-defined nanocomposite was employed to determine the 4 target metal ions. Isolated peaks at approximately 0.24, -0.6, -0.8 and -0.1 V for Hg(II), Pb(II), Cd(II) and Cu(II) were observed when all species coexisted. As reported in previous literature, the formation of an intermetallic compound may result in decreases of the peaks for

both Hg(II) and Cu(II). The voltammetric peaks were separated enough, and the electrode of the ZnO/RGO nanocomposite was feasibly employed for selective and simultaneous detection. The resultant calibration curves of Hg(II), Pb(II), Cd(II) and Cu(II) were established from 1.2 to 0.3 μM. The resulting LODs of Hg(II), Pb(II), Cd(II) and Cu(II) were identified as 0.06, 0.03, 0.04 and 0.03 μM, respectively. Compared with the standards set by the World Health Organization (WHO), the resulting LODs are lower than the guideline values.

Interference of other metal ions with the detection of at ZnO/RGO modified GCE was examined. Different chemical species, including Ca^{2+}, Co^{2+}, Cr^{3+}, Mn^{2+}, Ni^{2+}, Zn^{2+}, SO_4^{2-}, Cl^-, NO_3^{2-}, NO_2^- and ClO_4^-, at 1 μM, had no significant influence on the signals of 0.5 μM each of Hg (II), Pb (II), Cd (II) and Cu (II) with deviations below 5.0%. As the results showed, the electrode is highly selective for the simultaneous determination of Hg (II), Pb (II), Cd (II) and Cu (II) in the presence of different cations and anions. The repeatability of the electrode was investigated by repetitively determining the mixed solution containing 0.5 μM each of Hg (II), Pb (II), Cd (II) and Cu (II). It was found that the relative standard deviations (RSD) of peak currents for the four metal ions were 1.7% for Hg^{2+}, 2.4% for Pb^{2+}, 2.1% for Cd^{2+} and 3.1% Cu^{2+}.

4. CONCLUSIONS

A hydrothermal one-pot method was employed to fabricate a new ZnO/RGO nanocomposite. A GCE functionalized by the ZnO/RGO nanocomposite was successfully used to selectively determine different heavy metal ions. The obtained results indicate this novel nanocomposite of ZnO/RGO, which contains the advantages of ZnO as well as graphene, is a potential material to electrochemically detect heavy metal ions. Various potentials of separated stripping peaks were achieved for Hg(II), Pb(II), Cd(II) and Cu(II) on the nanocomposite of ZnO/RGO. Compared with the standards set by the World Health Organization (WHO), the resulting LODs are lower than the guideline values.

References

1. I. Turyan and D. Mandler, *Nature*, 362 (1993) 703.
2. H.P. Wu, *Anal. Chem.*, 68 (1996) 1639.
3. J. Van Staden and M. Matoetoe, *Anal. Chim. Acta.*, 411 (2000) 201.
4. Y. Bonfil, M. Brand and E. Kirowa-Eisner, *Anal. Chim. Acta.*, 464 (2002) 99.
5. X. Dai, O. Nekrassova, M.E. Hyde and R.G. Compton, *Anal. Chem.*, 76 (2004) 5924.
6. G. Aragay, J. Pons and A. Merkoçi, *Journal of Materials Chemistry*, 21 (2011) 4326.
7. M. Pumera, A. Ambrosi, A. Bonanni, E.L.K. Chng and H.L. Poh, *TrAC Trends in Analytical Chemistry*, 29 (2010) 954.
8. D. Du, J. Liu, X. Zhang, X. Cui and Y. Lin, *Journal of Materials Chemistry*, 21 (2011) 8032.
9. G. Williams, B. Seger and P.V. Kamat, *ACS nano*, 2 (2008) 1487.
10. C. Xu, X. Wang and J. Zhu, *J Phys Chem C*, 112 (2008) 19841.
11. J. Liu, S. Fu, B. Yuan, Y. Li and Z. Deng, *Journal of the American Chemical Society*, 132 (2010) 7279.
12. Y. Si and E.T. Samulski, *Chemistry of Materials*, 20 (2008) 6792.
13. J. Li, S. Guo, Y. Zhai and E. Wang, *Anal. Chim. Acta.*, 649 (2009) 196.

14. J. Li, S. Guo, Y. Zhai and E. Wang, *Electrochemistry Communications*, 11 (2009) 1085.
15. J. Gong, T. Zhou, D. Song and L. Zhang, *Sensors and actuators B: Chemical*, 150 (2010) 491.
16. S. Pearton, D. Norton, K. Ip, Y. Heo and T. Steiner, *Superlattices and Microstructures*, 34 (2003) 3.
17. V. Khranovskyy, R. Minikayev, S. Trushkin, G. Lashkarev, V. Lazorenko, U. Grossner, W. Paszkowicz, A. Suchocki, B.G. Svensson and R. Yakimova, *Journal of Crystal Growth*, 308 (2007) 93.
18. M.H. Huang, Y. Wu, H. Feick, N. Tran, E. Weber and P. Yang, *Adv. Mater.*, 13 (2001) 113.
19. V. Khranovskyy, I. Tsiaoussis, G. Yazdi, L. Hultman and R. Yakimova, *Journal of Crystal Growth*, 312 (2010) 327.
20. Z.W. Pan, Z.R. Dai and Z.L. Wang, *Science*, 291 (2001) 1947.
21. S.J. Pearton, F. Ren, Y.-L. Wang, B. Chu, K. Chen, C. Chang, W. Lim, J. Lin and D. Norton, *Progress in Materials Science*, 55 (2010) 1.
22. A. Taherkhani, T. Jamali, H. Hadadzadeh, H. Karimi-Maleh, H. Beitollahi, M. Taghavi and F. Karimi, *Ionics*, 20 (2014) 421.
23. S. Xu, L. Fu, T.S.H. Pham, A. Yu, F. Han and L. Chen, *Ceram. Int.*, 41 (2015) 4007.
24. B. Li, T. Liu, Y. Wang and Z. Wang, *Journal of colloid and interface science*, 377 (2012) 114.
25. M. Ahmad, E. Ahmed, Z.L. Hong, N.R. Khalid, W. Ahmed and A. Elhissi, *J. Alloy. Compd.*, 577 (2013) 717.
26. H. He, J. Klinowski, M. Forster and A. Lerf, *Chemical physics letters*, 287 (1998) 53.
27. A. Lerf, H. He, M. Forster and J. Klinowski, *J Phys Chem B*, 102 (1998) 4477.
28. F. Li, J. Song, H. Yang, S. Gan, Q. Zhang, D. Han, A. Ivaska and L. Niu, *Nanotechnology*, 20 (2009) 455602.
29. Y. Wei, L.-T. Kong, R. Yang, L. Wang, J.-H. Liu and X.-J. Huang, *Chemical Communications*, 47 (2011) 5340.
30. A. Afkhami, H. Ghaedi, T. Madrakian and M. Rezaeivala, *Electrochimica Acta*, 89 (2013) 377.
31. J.J. Yang, F. Miao, M.D. Pickett, D.A. Ohlberg, D.R. Stewart, C.N. Lau and R.S. Williams, *Nanotechnology*, 20 (2009) 215201.
32. L. Xiao, B. Wang, L. Ji, F. Wang, Q. Yuan, G. Hu, A. Dong and W. Gan, *Electrochimica Acta*, 222 (2016) 1371.
33. H. Dai, N. Wang, D. Wang, H. Ma and M. Lin, *Chem. Eng. J.*, 299 (2016) 150.
34. H. Bagheri, A. Hajian, M. Rezaei and A. Shirzadmehr, *J. Hazard. Mater.*, 324 (2017) 762.
35. L. ÖZcan, M. Altuntas, A. BÜYÜKsagis, T. Hayrettin and S. Yurdakal, *Analytical Sciences*, 32 (2016) 881.
36. L. Xiao, H. Xu, S. Zhou, T. Song, H. Wang, S. Li, W. Gan and Q. Yuan, *Electrochimica Acta*, 143 (2014) 143.
37. H. Xu, L. Zeng, S. Xing, Y. Xian, G. Shi and L. Jin, *Electroanalysis*, 20 (2008) 2655.
38. D. Li, J. Jia and J. Wang, *Talanta*, 83 (2010) 332.
39. L. Zhu, C. Tian, R. Yang and J. Zhai, *Electroanalysis*, 20 (2008) 527.